Supplemental Material for "Entanglement – nonstabilizerness separation in hybrid quantum circuits"

Gerald E. Fux [1] Emanuele Tirrito [1,2] Marcello Dalmonte [1,3] and Rosario Fazio [1,4]

[1] *The Abdus Salam International Center for Theoretical Physics (ICTP), Strada Costiera 11, 34151 Trieste, Italy*
[2] *Pitaevskii BEC Center, CNR-INO and Dipartimento di Fisica, Università di Trento, Via Sommarive 14, Trento, I-38123, Italy*
[3] *Scuola Internazionale Superiore di Studi Avanzati (SISSA), Via Bonomea 265, 34136 Trieste, Italy*
[4] *Dipartimento di Fisica "E. Pancini", Università di Napoli "Federico II", Monte S. Angelo, I-80126 Napoli, Italy*

(Dated: September 19, 2024)

We present additional information on (1) the properties of the stabilizer entropy, (2) the tensor network computations, (3) the extraction of the critical measurement rates, (4) the scaling collapse, (5) an analogous setup with T-gates replaced by CCZ-gates, (6) a conjectured phase diagram in p vs. η for $\beta = 1$, (7) a conjectured phase diagram in p vs. β for $\eta = 1$, and (8) an argument for coincident entanglement and nonstabilizerness transitions.

1. Properties of the stabilizer entropy

The stabilizer Rényi entropy is a recently introduced nonstabilizerness monotone [1]. It can be computed numerically even for a large number of qubits [2–4] and is also experimentally accessible [5]. In this section, we briefly state some of its key properties to allow easy access to the main results of the paper.

For three common choices of α, the stabilizer Rényi entropy [as defined in Eq. (2) of the main text] reads

$$\mathcal{M}_\alpha(|\psi\rangle) = \begin{cases} \log_2\left(|\{P \in \mathcal{P}_N : \langle P\rangle_\psi \neq 0\}|\right) - N & \alpha \to 0 \\ -\sum_P 2^{-N}\langle P\rangle_\psi^2 \log_2\left(\langle P\rangle_\psi^2\right) & \alpha \to 1 \\ -\log_2\left(\sum_P 2^{-N}\langle P\rangle_\psi^4\right) & \alpha = 2 \end{cases} \tag{S1}$$

where $P \in \mathcal{P}_N$ is the group of all N–qubit Pauli strings with $+1$ phases. We list some key properties of the stabilizer α–Réney entropies, alongside the references that contain the respective proofs:

(i) *Faithfulness*: $\mathcal{M}_\alpha(|\psi\rangle) = 0$ if and only if $|\psi\rangle$ is a stabilizer state (see Ref. [1]).

(ii) *Stability under free operations*: For any unitary Clifford operator C and state $|\psi\rangle$ it holds that $\mathcal{M}_\alpha(C|\psi\rangle) = \mathcal{M}_\alpha(|\psi\rangle)$ (see Ref. [1]).

(iii) *Additivity*: $\mathcal{M}_\alpha(|\psi\rangle \otimes |\phi\rangle) = \mathcal{M}_\alpha(|\psi\rangle) + \mathcal{M}_\alpha(|\phi\rangle)$ (see Ref. [1]).

(iv) *Bounded*: For any N-qubit state $|\psi\rangle$ it holds that $0 \leq \mathcal{M}_\alpha(|\psi\rangle) < N$ (see Ref. [1]).

(v) $M_{\alpha'}(|\psi\rangle) < \mathcal{M}_\alpha(|\psi\rangle)$ for $\alpha' > \alpha$ (see Ref. [6]).

(vi) The stabilizer entropies consitute a lower bound to the so-called T–count $t(|\psi\rangle)$ of a state: $\mathcal{M}_\alpha(|\psi\rangle) < t(|\psi\rangle)$ (see Ref. [7]).

(vii) For $\alpha > 1/2$ the stabilizer entropies constitute a lower bound to the so-called "robustness of magic": $\mathcal{M}_\alpha(|\psi\rangle) < \mathcal{R}_\psi$ (see Refs. [1, 8]).

2. Tensor network computations

Figures 3 and 4 in the main text are based on tensor network calculations of 512 trajectories for each combination of various T-gate scaling prefactors η, measurement rates p, and system sizes N. The sets of possible values are $\eta \in \{0.5, 1.0, 2.0, 4.0, 8.0\}$, $p \in \{0.14, 0.16, \ldots, 0.34\}$, and $N \in \mathcal{N} = \{8, 12, 16, 24, 32, 48, 64, 92, 128, 184\}$, where we however exclude $N \in \{92, 128, 184\}$ for $p \in \{0.14, 0.16\}$. All computations assume $\beta = 1$. We start each trajectory in the $|00\ldots0\rangle$ state and evolve it as a matrix product state (MPS) using the Julia language version of the tensor network package iTensor [9, 10]. Each of the random 2-site Clifford gates are generated independently by 30 alternating layers of a random choice of (1) random single site Clifford gates, (2) the swap operation, (3) the controlled-not operation acting on the left qubit, and (4) the controlled-not operation acting on the right qubit. The single site Clifford gates are directly sampled from the 24 different gates of the Clifford group. As a singular value truncation strategy we use a combination of both a relative and an absolute threshold of $\epsilon = 10^{-6}$ and $\chi = 256$, respectively. To check convergence with respect to these thresholds we have performed the same computations (for a subset of parameter sets) substituting the thresholds with $\epsilon = 10^{-5}$ and $\chi = 128$. We found that the results did not change significantly compared to the errors due to the statistics of the finite number of trajectories.

For every qubit and every time step we independently apply a T-gate with probability $q = \eta/N^\beta$. The application of a measurement occurs analogously with probability p. The outcome of each measurement is, however, weighted by the Born rule and we renormalize the state after the projection.

At every 8^{th} time step we compute the Schmidt coefficients between the left and the right half of the chain, as well as the Pauli string distribution. The Schmidt coefficients are obtained by bringing the orthogonality center

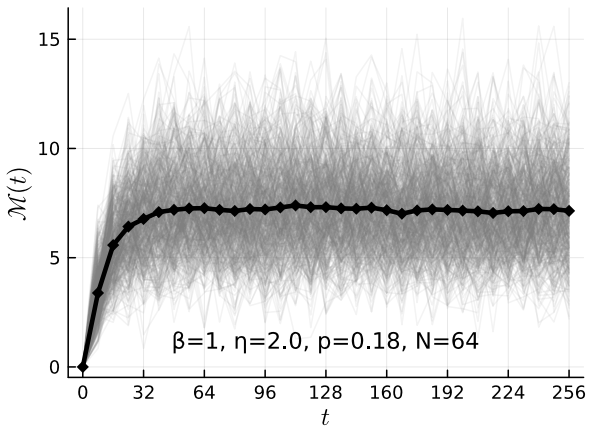

FIG. S1. Time evolution of the stabilizer 2-Rény entropy $\mathcal{M}(t)$ of 512 trajectories (gray lines) and their average (thick solid black line).

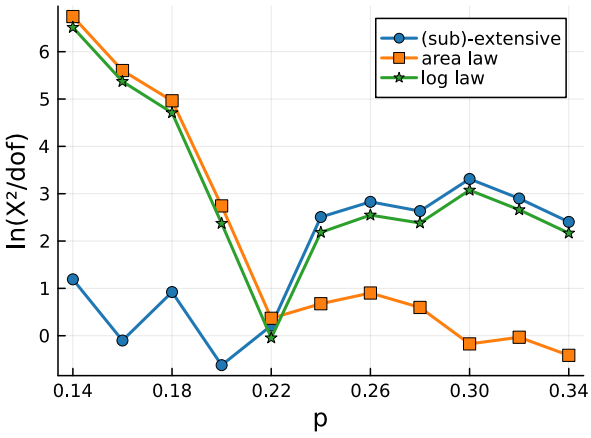

FIG. S2. The squared residuals per degree of freedom as a function of the measurement rate p for the nonstabilizerness of a hybrid circuit with T-gate density $q = \eta/N^\beta$, where $\eta = 2.0$ and $\beta = 1.0$.

of the MPS to site $N/2$ and performing a singular value decomposition between site $N/2$ and $N/2+1$. To obtain the Pauli string distribution we implement the method explained in [3]. We found that a sample size of 128 Pauli strings is sufficient for a good estimate of the stabilizer 2-Rény entropy. From the Schmidt coefficients and the Pauli string distribution we calculate the von-Neumann entropy $\mathcal{E}(t)$ and the stabilizer 2-Rény entropy $\mathcal{M}(t)$.

In Fig. S1 we show the 512 trajectories of $\mathcal{M}(t)$ as gray lines and their average $\bar{\mathcal{M}}(t)$ for $\eta = 2.0$, $p = 0.18$, and $N = 64$. We can see that $\bar{\mathcal{M}}(t)$ reaches a steady state after about 50 time steps for these parameters. For all parameter sets considered in this paper we find that the approximate steady state is reached before $t = 2N$ time steps. To extract the approximate steady state value of $\bar{\mathcal{M}}(t)$ and $\bar{\mathcal{E}}(t)$ we average over all values of $\mathcal{M}(t)$ and

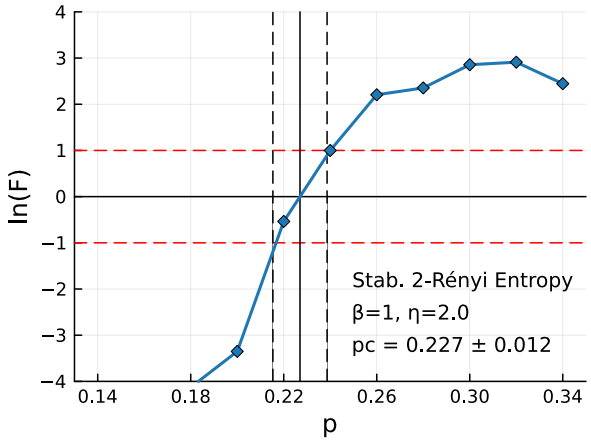

FIG. S3. The logarithm of F as a function of the measurement rate p for the nonstabilizerness of a hybrid circuit with T-gate density $q = \eta/N^\beta$, where $\eta = 2.0$ and $\beta = 1.0$. The blue diamond symbols show $\ln[F(p)]$ calculated for the discrete set of computed measurement rates p and the solid blue line shows a linear interpolation. The vertical solid black line shows the extracted critical measurement rate p_c. The vertical dashed black lines indicates the estimated error σ_{p_c}.

$\mathcal{E}(t)$ from time $t = 2N$ to $t = 4N$. Because we have each one value of $\bar{\mathcal{M}}(t)$ and $\bar{\mathcal{E}}(t)$ for every 8^{th} time step this means that the approximate steady states $\bar{\mathcal{M}}_{\text{ss}}$ and $\bar{\mathcal{E}}_{\text{ss}}$ are determined as an average over $P = N/4$ values. The error bar for each of these approximate steady states shown in Fig. 3 of the main text is the standard deviation of this distribution. The computations were performed on the Cineca HPC Marconi cluster with 2×24-cores Intel Xeon 8160 CPUs and consumed a total of 36k CPUh.

3. Extraction of critical measurement rates

As explained in the main text we fit the data computed in the previous section to the function $f(N) = a + bN^\gamma$ with the constraint that $\gamma > 0$ for the power law and $\gamma \leq 0$ for a function that approaches a constant, to see which law fits the data best. For each curve and fitting function we perform a weighted least square fit and extract the squared residuals per degree of freedom χ^2/dof, where

$$\chi^2 = \sum_{N\in\mathcal{N}} \frac{\bar{\mathcal{M}}_{\text{ss}}(N) - f(N, a_{\text{fit}}, b_{\text{fit}}, \gamma_{\text{fit}})}{\sigma(N)}, \tag{S2}$$

with the computed steady state expectation value of nonstabilizerness $\bar{\mathcal{M}}_{\text{ss}}(N)$ and the error $\sigma(N)$ of each data point. The degree of freedom (dof) is the number of data points minus the number of fit parameters. We find that using the standard deviation computed above often leads to a $\chi^2/\mathsf{dof} \simeq 0.05$ which signals that we have overestimated the error. Assuming that the distribution of averaged values from time $t = 2N$ to $t = 4N$ is approxi-

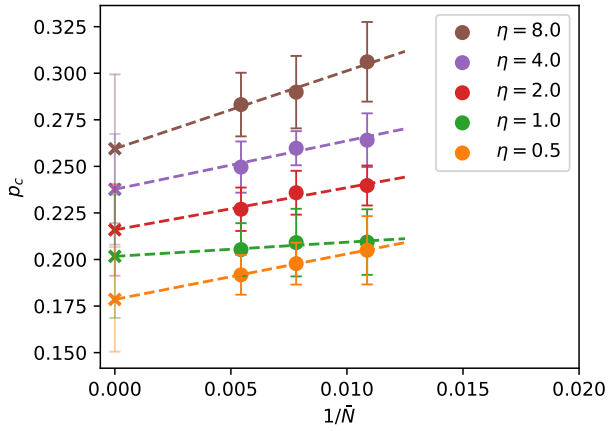

FIG. S4. Linear extrapolation of F-test results for p_c of the nonstabilizerness transition. The circles mark the F-test results as a function of $1/\bar{N}$, where $\bar{N}$ are the largest system sizes included in the data.

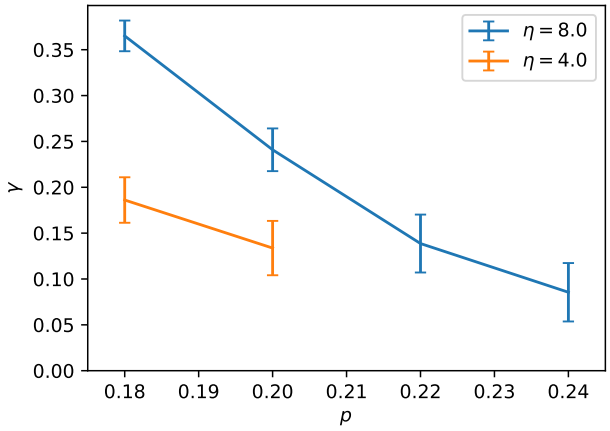

FIG. S5. Extrapolated power law exponent γ for the nonstabilizerness in phase II for $\beta = 1$.

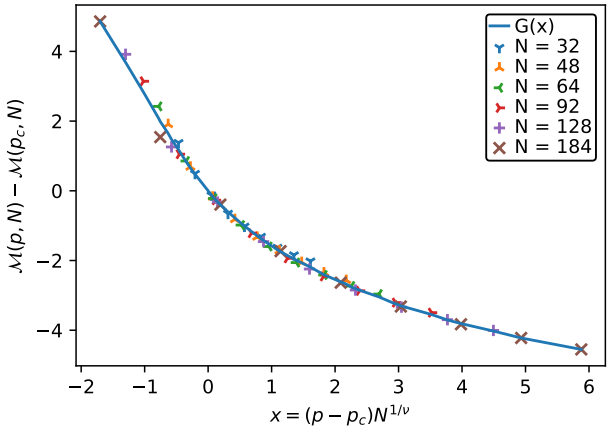

FIG. S6. Scaling collapse of nonstabilizerness $\mathcal{M}(p, N)$ data for T-gate prefactor $\eta = 2.0$, multiple system sizes N, and multiple measurement rates p, assuming a critical measurement rate of $p_c = 0.216$. For this data and assumed p_c we find an optimal critical exponent of $\nu = 1.35$.

mately uncorrelated, the standard deviation needs to be rescaled by a factor of $1/\sqrt{P}$. In Fig. S2 we plot χ^2/dof against the measurement rate p for the power law and the constant fit functions using the rescaled standard deviation. In addition to this, we also plot χ^2/dof for fits of a logarithmic scaling function $f_{\log}(N) = a + b\ln(N)$. For each fit we use the data points corresponding to the 7 largest available system sizes. We can clearly see that for small measurement rates the power law scaling fits the data best, while at large rates the function approaching a constant fits best. Moreover, using the rescaled standard deviation, for all p the best fits have a χ^2/dof close to the optimal value of 1. To extract the critical measurement rate we plot in Fig. S3 the logarithm of

$$F(p) = \frac{E_{\text{ext}}(p)}{E_{\text{area}}(p)}, \tag{S3}$$

which is the ratio of $E(p) = \chi^2/\mathsf{dof}$ for the power law and constant scaling fits. We connect the discrete data points with a linear interpolation and quote the measurement rate at which $\ln[F(p_c)] = 0$ as the critical measurement rate p_c. We estimate the error of this value to be $(p^+ - p^-)/2$ where $p^\pm$ are such that $\ln[F(p^\pm)] = \pm 1$. Finally, to mitigate finite size effects we redo this extraction of p_c with restricted data only including steady state values up to a system size of $\bar{N} = 92, 128, 184$. We plot the results against $1/\bar{N}$ in Fig. S4, and extrapolate the obtained values towards $1/\bar{N} \to 0$ with a linear fit. The same analysis is done independently for both nonstabilizerness and entanglement, and for different T-gate density prefactors η. Figure 4 in the main text summarizes the results of these calculations.

Finally, we extrapolate the power law exponents γ for the available data in phase II to $1/\bar{N} \to 0$ in a similar way as done for p_c in Fig. S4, and plot the result in Fig. S5. We find that the power law exponent appears to depend on the distance to the phase boundary between phase II and phase III.

4. Scaling collapse

To confirm the critical nature of the measurement rates for the nonstabilizerness transition extracted through the above analysis we perform a scaling collapse. For a given p_c and exponent ν we plot $\mathcal{M}(p, N) - \mathcal{M}(p_c, N)$ against $x = (p - p_c)N^{1/\nu}$. We then fit a piecewise linear function $G(x)$ to the data in the same way as explained in detail in appendix A of Ref. [11]. For each value of η and p_c we compute in this way the optimal exponent ν. Figure S6 shows an example of such an optimal scaling collapse for $\eta = 2.0$ and $p_c = 0.216$ which results in an optimal exponent of $\nu = 1.35$.

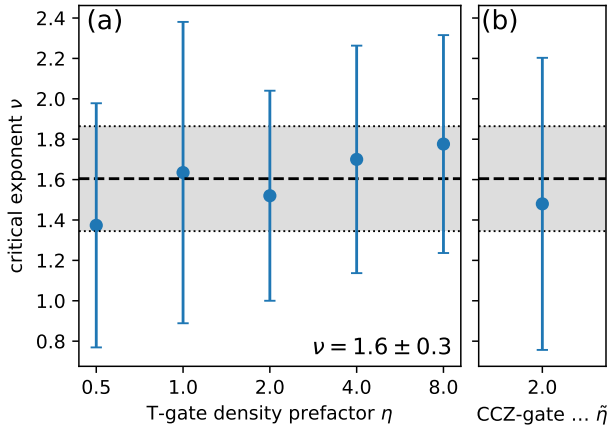

FIG. S7. Extracted critical exponent of the non-stabilizer phase transition for (a) various T-gate density prefactors η and (b) CCZ-gate density prefactor $\tilde{\eta}$. A constant fit to the T-gate case values results in an overall critical exponent estimate of $\nu = 1.6 \pm 0.3$ (indicated as the gray shaded region).

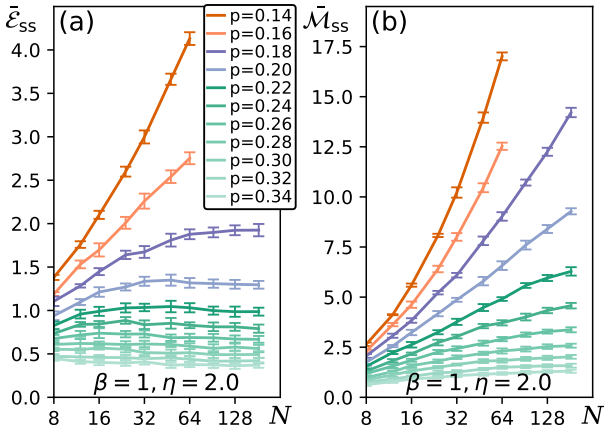

FIG. S8. Numerical results for the average steady state entanglement (a) and nonstabilizerness (b) versus system size N for several different measurement rates p and CCZ-gate density $q(N) = \eta/N^{\beta}$ with $\eta = 2.0$ and $\beta = 1$.

In Fig. S7(a) we show the exponents ν that result from the critical measurement rates for different T-gate prefactors η presented in Fig 4. For each η the expected value and standard deviation of ν is calculated from the distribution of p_c, which is assumed to be Gaussian with a width given by the estimated error. Although the critical values p_c systematically increase with larger values of η, the critical exponent appears to land consistently at 1.6 ± 0.3. This confirms the expectation that the critical rates may depend on the details of a model but critical exponents do not.

5. Monitored Clifford circuits interspersed with CCZ-gates

To showcase the generality of the above model and motivated by a recent experiment [12] we repeat the entire analysis (for $\eta = 2.0$) replacing T-gates with CCZ-gates. Figure S8 shows the average steady state entanglement and nonstabilizerness for this CCZ-gate doped circuit (analogous to Fig. 3 of the main text). While one expects that the details of the nonstabilizerness phase transition, such as the critical rate p_c, may depend on such details of the circuit, we expect that the nature of the transition, reflected in the critical exponent ν, is the same. Performing the F-test and scaling collapse presented above yields results consistent with this expectation. While the critical measurement rate for the nonstabilizerness transition is different from the corresponding T-gate case, the critical exponent does not change significantly, as shown in Fig. S7(b).

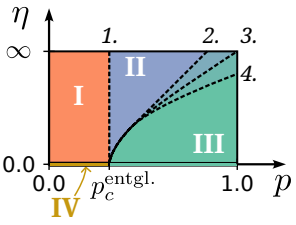

FIG. S9. Sketch of a conjectured phase diagram (p vs. η) for $\beta = 1$. The roman numbered phases correspond to the phases introduced in the main text. The four black dashed lines mark the nonstabilizerness phase transitions in four different scenarios listed in the text. In scenario 1 the entanglement and nonstabilizerness phase transition would coincide for all η and phase II would thus completely disappear.

6. Conjectured phase diagram for p vs. η

To complete the phase diagram of Fig. 4 of the main text, we discuss the sketch of a speculative phase diagram for the full range of $\eta \in [0, \infty)$ with $\beta = 1$ shown in Fig. S9.

A first non-trivial question is the limit of $\eta \to 0^+$, for which we would conjecture that both phase transitions merge to coincide at $p_c^{\text{entgl.}}$, following the argument laid out in section "8. Argument for coincident entanglement and nonstabilizerness transitions" below. Here $p_c^{\text{entgl.}} = 0.15995(10)$ is the critical measurement rate of the entanglement phase transition in the pure Clifford circuit (i.e. $\eta = 0$) [13, 14]. This would imply that from $\eta \to 0^+$ to $\eta = 0$ the nonstabilizerness makes a discontinuous jump from a power law to zero for $p < p_c^{\text{entgl.}}$. Then, for finite values of η, our numerical results suggests a shift of the nonstabilizerness transition while the entanglement phase transition stays unchanged. Again, the arguments laid out in section 8 below would suggest

that the transitions coincide and both stay unchanged. However, compared to the $\eta \to 0^+$ case the argument appears to be applicable only with additional caveats.

Finally, for $\eta \to \infty$ there are at least four different plausible scenarios:

1. The argument laid out in section 8 is applicable for all values of η and hence both phase transitions coincide for the entire phase diagram (removing the occurrence of phase II completely).
2. The critical measurement rate for the nonstabilizerness transition approaches a finite value (i.e. smaller 1) for $\eta \to \infty$.
3. The critical measurement rate for the nonstabilizerness transition approaches 1 only at $\eta \to \infty$.
4. The critical measurement rate for the nonstabilizerness transition approaches 1 already for a finite value of η.

We indicate all four scenarios in Fig. S9.

7. Conjectured phase diagram for p vs. β

A natural question following from the results for $\beta = 1$ from the main text is whether the non-trivial phase transition we observe persists for a T-gate density that vanishes as η/N^β even if $\beta \neq 1$. As a first attempt to answer this question we consider a simple hybrid quantum circuit identical to the circuit considered above but with the two qubit brickwork structure replaced by only single site random Clifford gates. In this scenario the total state is always a product state of single qubits. This allows straight forward analytical considerations that (for $\beta > 0$) yield

$$\bar{\mathcal{M}}_{\rm ss}(N \to \infty) = \eta\, \bar{\mathcal{M}}_1\, \frac{1-p}{p}\, N^{1-\beta}, \tag{S4}$$

where $\bar{\mathcal{M}}_1$ is the average nonstabilizerness of a random single site stabilizer state after the application of a single T-gate. Hence, assuming a non-trivial measurement rate $0 < p < 1$, we find a power law for $0 < \beta < 1$, a p dependent constant for $\beta = 1$, and a vanishing nonstabilizerness for $1 < \beta$. Figure S10(a) shows the phase diagram for this simple product Clifford circuit.

Figure S10(b) shows a speculative phase diagram for the full quantum circuit (including the two qubit Clifford brickwork structure) at fixed $\eta = 1.0$, for which only the $\beta = 1.0$ line has been studied numerically in this work so far. We lay out some heuristic arguments for this phase diagram in the following, which—we would like to stress—is only intended to serve as a starting point for further analysis and discussions.

We start with the entanglement phase transition, which we draw to be independent of β because we do not expect that the sub-extensive density of T-gates for

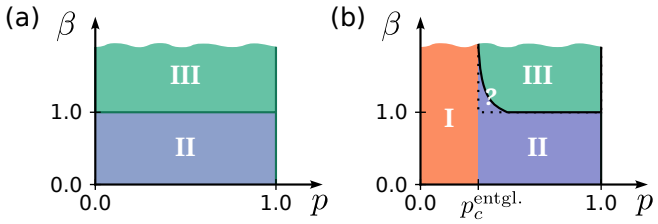

FIG. S10. Phase diagram (p vs. β) for the separable hybrid quantum circuit (a) and a sketch of a conjectured phase diagram for the full hybrid quantum circuit (b). The roman numbered phases correspond to the phases introduced in the main text. While our numerical results suggest that there is an immediate phase II between phase I and III for $\beta = 1$ for the full circuit, another argument explained in section 8 suggests a direct transition from I to III (dotted line).

$\beta > 0$ changes the entanglement phase transition compared to the pure Clifford case. Furthermore, for $\beta = 0$, i.e. an extensive number of T-gates per layer, the setup may be understood as a proxy to Haar-random circuits, for which an equal critical measurement rate would be still consistent with the known results in the literature.

Next we discuss the nonstabilizerness for $\beta < 1$. We conjecture that all cases with $p < 1$ and $\beta < 1$ will lead to a power law in nonstabilizerness. For this we have the following argument. Consider the stabilizer Rényi entropy after a single layer of Clifford gates, T-gates, and measurements, under the assumption of $\eta > 0$, $p < 1$, and $\beta < 1$. As the density of T-gates is $q = \eta/N^\beta$, there will on average be a number of $\eta N^{1-\beta}$ T-gates in the first layer. The application of measurements will then effectively remove a p fraction of them, leaving $\eta(1-p)N^{1-\beta}$ effective T-gates in the first layer. As the state on which the T-gates act is a product state of paired qubits, each T-gate will contribute separately to the total stabilizer Rényi entropy, which follows from its additive property. Hence after the first step the averaged stabilizer Rényi entropy grows from $\bar{\mathcal{M}} = 0$ to $\bar{\mathcal{M}} \propto \eta(1-p)N^{1-\beta}$. It appears reasonable to assume (though technically not guaranteed) that the application of further Clifford, T-gate, and measurement layers will not decrease the averaged value of $\bar{\mathcal{M}}$. Hence, the long time limit of $\bar{\mathcal{M}}$ would then scale at least as $O(N^{1-\beta})$, which for $\beta < 1$ then falls into the category of the power law phase.

For $\beta > 1$, on the other hand, it might be that the effect of T-gates decays slow enough to counteract the dilute doping of the circuit with T-gates. Assume, for example, that for low enough measurement rates the nonstabilizerness induced by a T-gate permeates through the circuit and persists for times of order $\exp(N)$. In Ref. [15] this is indeed argued to be the case for $p < p_c^{\rm entgl.}$. Then, even with the very dilute density of T-gates $q = \eta/N^\beta$ with $\beta > 1$, it would take only $O(N^{\beta+\alpha-1})$ time steps with $\alpha > 0$ to potentially reach a state with $\mathcal{M} \propto O(N^\alpha)$. This means that even for $\beta > 1$ the nonstabilizerness

could indeed still follow a power law for low enough measurement rates.

Finally for $\beta = 1$, our numerical results suggest that the entanglement and nonstabilizerness phase transitions are separate as drawn in the conjectured phase diagram in Fig. S9. We note, that the argument laid out in section 8 would on the other hand suggest that they should coincide, which we indicate with the dotted black line in Fig. S9.

8. Argument for coincident entanglement and nonstabilizerness transitions

For completeness, we would like to conclude by pointing also at a different scenario that cannot be rule out by our work. Despite the finite scaling analysis, the $1/N \to 0$ extrapolation, and the conservative error estimation carried out in this numerical study, finite size effect may nonetheless play a role leading the entanglement and nonstabilizerness transitions to coincide.

An approximate argument for why the nonstabilizerness phase transition could be indeed independent of η and coincident with the entanglement phase transition has been put forward in Ref. [15] and goes as follows. Consider the averaged nonstabilizerness of a brickwork Clifford circuit with projective measurements (with probability p) and only a single interspersed T-gate. In this setup one finds a dynamical phase transition between a phase where the nonstabilizerness decays like $\exp(-t/\tau)$ with $\tau \propto \exp(N)$ for $p < \tilde{p}_c$ and a phase where the decay time τ is independent of N for $p > \tilde{p}_c$. Hence, for $p > \tilde{p}_c$ the impact of a T-gate onto a stabilizer state vanishes at a constant time scale of order τ. Because the average distance in space-time between nearest two T-gates in our proposed setup for $\beta = 1$ is $\sqrt{N/\eta}$ this means that for $p > \tilde{p}_c$ the impact of each T-gate typically decays independently before overlapping with any other T-gate for $N \to \infty$. This would then imply an overall constant scaling of nonstabilizerness for $p > \tilde{p}_c$, independently of η. The above argument relies on the crucial assumption that T-gates not only have minimal space-time overlap, but their overlap is not affecting the dynamics. This implies that their rare-event statistics is irrelevant. Our numerical results point to a different scenario, where such rare events *are* relevant and make the two phase transitions distinct, while still satisfying the restriction theorem put forward in Ref. [16]. This scenario is perfectly compatible with the numerical simulations reported in Ref. [15], as they concern highly nonequivalent witnesses of nonstabilizerness. It would be interesting to understand which physical scenarios lead to such rare events being relevant, and which ones do not.

[1] L. Leone, S. F. E. Oliviero, and A. Hamma, Stabilizer rényi entropy, Phys. Rev. Lett. **128**, 050402 (2022).
[2] T. Haug and L. Piroli, Quantifying nonstabilizerness of matrix product states, Phys. Rev. B **107**, 035148 (2023).
[3] G. Lami and M. Collura, Quantum magic via perfect sampling of matrix product states (2023), arXiv:2303.05536.
[4] P. S. Tarabunga, E. Tirrito, T. Chanda, and M. Dalmonte, Many-body magic via Pauli-Markov chains – from criticality to gauge theories (2023), arXiv:2305.18541.
[5] S. F. E. Oliviero, L. Leone, A. Hamma, and S. Lloyd, Measuring magic on a quantum processor, NPJ Quantum Inf. **8**, 148 (2022).
[6] T. Haug and L. Piroli, Stabilizer entropies and nonstabilizerness monotones, Quantum **7**, 1092 (2023).
[7] A. Gu, L. Leone, S. Ghosh, J. Eisert, S. Yelin, and Y. Quek, A little magic means a lot (2023), arXiv:2308.16228.
[8] M. Heinrich and D. Gross, Robustness of magic and symmetries of the stabiliser polytope, Quantum **3**, 132 (2019).
[9] G. Vidal, Efficient simulation of one-dimensional quantum many-body systems, Phys. Rev. Lett. **93**, 040502 (2004).
[10] M. Fishman, S. R. White, and E. M. Stoudenmire, The ITensor Software Library for Tensor Network Calculations, SciPost Phys. Codebases , 4 (2022).
[11] B. Skinner, J. Ruhman, and A. Nahum, Measurement-induced phase transitions in the dynamics of entanglement, Phys. Rev. X **9**, 031009 (2019).
[12] D. Bluvstein, S. J. Evered, A. A. Geim, S. H. Li, H. Zhou, T. Manovitz, S. Ebadi, M. Cain, M. Kalinowski, D. Hangleiter, J. P. B. Ataides, N. Maskara, I. Cong, X. Gao, P. S. Rodriguez, T. Karolyshyn, G. Semeghini, M. J. Gullans, M. Greiner, V. Vuletić, and M. D. Lukin, Logical quantum processor based on reconfigurable atom arrays, Nature 10.1038/s41586-023-06927-3 (2023).
[13] Y. Li, X. Chen, and M. P. A. Fisher, Quantum zeno effect and the many-body entanglement transition, Phys. Rev. B **98**, 205136 (2018).
[14] P. Sierant, M. Schirò, M. Lewenstein, and X. Turkeshi, Measurement-induced phase transitions in (d + 1) -dimensional stabilizer circuits, Phys. Rev. B **106**, 214316 (2022).
[15] M. Bejan, C. McLauchlan, and B. Béri, Dynamical magic transitions in monitored clifford+t circuits, PRX Quantum **5**, 030332 (2024).
[16] A. Gu, S. F. Oliviero, and L. Leone, Magic-induced computational separation in entanglement theory (2024), arXiv:2403.19610.